The Astronomical Journal, 123:3298–3304, 2002 June

THE FIRST ORBITAL PERIOD FOR A DWARF NOVA IN A GLOBULAR CLUSTER: V101 IN M5

James D. Neill[1]
Department of Astronomy, Columbia University, Mail Code 5242, 538 West 120th Street, New York, NY 10027; neill@astro.columbia.edu

Michael M. Shara
Department of Astrophysics, American Museum of Natural History, 79th and Central Park West, New York, NY 10025; mshara@amnh.org

Adeline Caulet
Calypso Observatory, Kitt Peak Observatory, 950 North Cherry Avenue, Tucson, AZ, 85726; caulet@calypso.org

and

David A. H. Buckley
South African Astronomical Observatory, P.O. Box 9, Observatory 7935, Cape Town, South Africa; dibnob@saao.ac.za
Received 2002 January 14; accepted 2002 February 28

ABSTRACT

We report the first orbital period determination for a dwarf nova (DN) in a globular cluster: V101 in M5 has a period of 5.796 ± 0.036 hr. We derived this period from *I*-band photometry acquired with the Calypso Observatory High Resolution Camera operating with tip-tilt adaptive optics correction. Observations from the South African Astronomical Observatory in the *V* band were also analyzed and exhibit a periodic signal of the same period. This orbital period suggests that V101 has a secondary of mid to late K spectral type with $M_V = +8.2 \pm 0.5$. The predicted spectral type is consistent with previous spectral observations in quiescence, which show a fairly red continuum. From the observed minimum brightness of $V = 22.5$, we derive a distance modulus of $(m - M)_V = 14.3 \pm 0.5$ to the DN, which supports V101's membership in the globular cluster M5. Measurement of the ellipsoidality effect indicates that the orbital plane of the V101 system is moderately inclined, but not enough to exhibit eclipses.

Key words: binaries: eclipsing — globular clusters: individual (M5) — novae, cataclysmic variables

On-line material: machine-readable tables

1. INTRODUCTION

Close binaries in globular clusters contain a significant fraction of the total binding energy of the clusters. This makes them critically important in unraveling the dynamical evolution of their host clusters. In order to place constraints on cluster evolution theory, one must determine the binding energy of the binaries in a cluster, i.e., their orbital periods and component masses. Determining the evolutionary states of cluster binaries is also important, and this also demands component masses and periods. The high stellar densities in the cores of many globular clusters, where most of the close binaries reside, make this an observational challenge. UV and X-ray observations have improved our population census of cluster close binaries (Knigge et al. 2002; Grindlay et al. 2001; Pooley et al. 2002), but without knowing the periods of these new binaries we cannot calculate the binding energy they contain or constrain their evolutionary state.

The cataclysmic variable (CV) V101 in the globular cluster M5 has many properties that make it an ideal candidate for period determination. It lies 280″ from the center of M5 (10 core radii) and is relatively uncrowded compared with the objects near the core of a globular cluster (see Fig. 1). It is classified as a dwarf nova (DN), a particularly well-studied class of CV for which empirical relations exist relating the period to the luminosity, spectral type, and mass of the secondary.

The literature on M5 V101 is not extensive. It was first reported as a possible SS Cyg type variable star by Oosterhoff (1941). He reported seven observations, including two pairs of measurements in outburst separated by 66 days in 1934. Since then Margon, Downes, & Gunn (1981) performed the initial identification of V101 in quiescence and obtained a low-resolution spectrum showing strong, broad Balmer and He I emission lines, confirming the identification and the DN classification. Shara, Potter, & Moffat (1987) reported *B*-band observations in outburst and quiescence and predicted a fairly long orbital period ($P \sim 11$ hr) based on the minimum observed magnitude ($V = 22.5$, Kukarkin & Mironov 1970) and the duration and rise and fall time of the outburst. Spectral observations of V101 in outburst were published by Naylor et al. (1989) and showed Hα in absorption with a fairly red continuum. They also showed a radial velocity curve covering 1.75 hr from which they concluded that the orbital period must be longer than twice their sampling interval ($P \geq 3.5$ hr, see their Fig. 2). Shara, Potter, & Moffat (1990) published the highest resolution spectrum to date of V101 in quiescence and noted that the high velocity width of the Balmer lines hinted that the system might be highly inclined and eclipses might be observable. The first X-ray detection was published by Hakala et al. (1997). They found V101 to be at the high end of the distribution of X-ray, luminosity for CVs in the galactic disk. They also classify V101 as a DN based on the ratio of X-ray to optical flux. Recent photometry showing two outbursts and the quiescent behavior of V101 are reported by Kaluzny et al. (1999).

The possibility of using eclipses to determine the orbital period for M5 V101 motivated this study. The availability

[1] Guest User, Canadian Astronomy Data Centre, which is operated by the Dominion Astrophysical Observatory for the Canadian National Research Council's Herzberg Institute of Astrophysics.

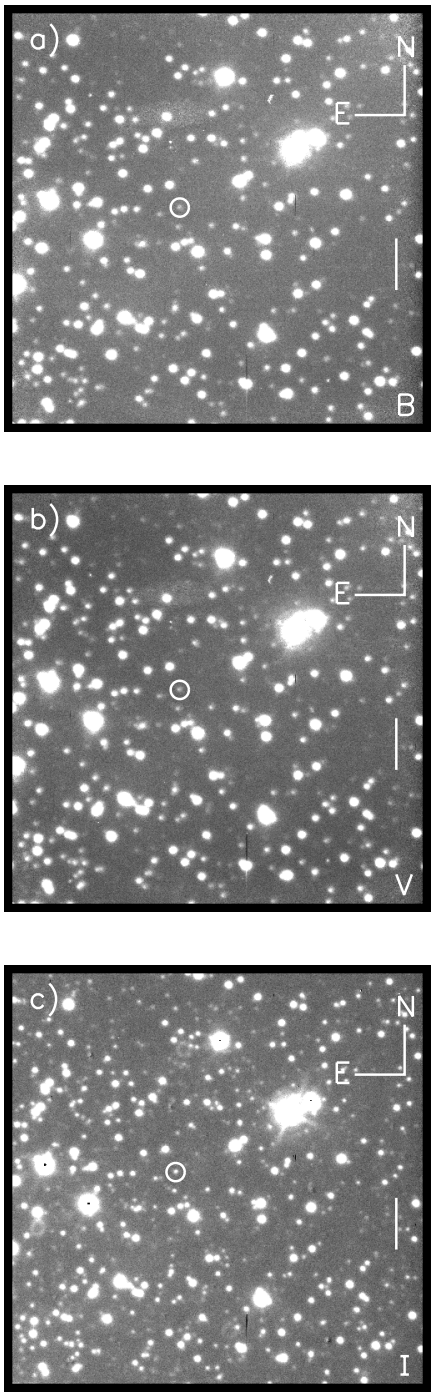

FIG. 1.—Calypso images of V101 produced by co-adding three 600 s HRCAM exposures. The scale bar on the right is 10″ long, and V101 is circled. (*a*) *B*-band data taken on JD 2,451,994 (26 March 2001) with a PSF that has a full width at half maximum (FWHM) of 0.″8. (*b*) *V*-band images taken on JD 2,451,993 (2001 March 25) with a PSF that has a FWHM of 0.″8. (*c*) *I*-band images taken on JD 2,452,051 (2001 May 22) with a PSF that has a FWHM of 0.″6.

of many nights on the Calypso Observatory 1.2 m telescope using the high-resolution camera allowed us to achieve the photometric accuracy and time sampling required to determine the orbital period. We now describe the photometric analysis and the method for finding the period, and we present the physical properties of V101 derived from our observations.

2. OBSERVATIONS

2.1. *Calypso Telescope Observations*

Since these are the first scientific results from the Calypso Telescope, we present a brief description of the telescope and camera. A more detailed description will be published elsewhere.

The Calypso Telescope is a 1.2 m telescope of Ritchey-Chrétien design on a computer-controlled altitude-azimuth mounting located on Kitt Peak, Arizona. Two instruments are mounted at the Naysmith foci: a high-resolution camera (HRCAM), with tip-tilt adaptive correction and a field of view of 85″, and a nonadaptive camera (WFCAM) with a 10′ field of view. The aperture of the telescope was matched to the atmospheric cell size during the best quartile of seeing at the site allowing the tip-tilt to theoretically correct 87% of the atmospheric distortion on the optical axis. The optical components are figured so that the total wave front error at the focal plane, including all error budgets, is less than 1/17 of a wavelength at 5500 Å. The telescope is mounted on a 10.2 m high pier with an enclosure that rolls completely away, allowing it to operate in the open air. The site is placed so the prevailing winds during the best seeing reach the telescope unhindered by any ground obstruction providing a laminar flow of air over the telescope.

The HRCAM was used for this study of V101. It uses a single Loral 2048^2 CCD with 15 μm pixels. Its native resolution is 0.″04 pixel^{-1} in order to oversample the point-spread function (PSF) at the best seeing measured at the site of 0.″25. However, the average seeing ranges between 0.″6 and 0.″8, as measured in the *I* band. Therefore, the CCD was binned 4×4 (giving a pixel size of 0.″16) to better accommodate these atmospheric conditions during the observing campaign. Since the secondary component of V101 was thought to be a late-type main-sequence (MS) star, we chose the *I* band to maximize the chances that ellipsoidal variations would be visible. We used 10 minute exposures back to back to allow us to sample the light curve densely enough to detect low-amplitude eclipses or ellipsoidal variations. This exposure time gave us a limiting magnitude of $I \sim 21.5$ under typical conditions. Table 1 presents the log of *I*-band observations for the Calypso data. Figure 1 presents three finder charts for V101 in the *B*, *V*, and *I* bands taken with the HRCAM on Calypso.

2.2. *South African Astronomical Observatory Observations*

Observations taken in 1995 with the Tek 4 CCD on the South African Astronomical Observatory (SAAO) 1.9 m telescope in the *V* band were also analyzed for this study. For five nights, V101 was observed with 15 minute exposures back to back over the entire night, yielding a limiting magnitude of $V \sim 22.7$ under typical conditions. Table 1 presents the log of observations for the SAAO *V*-band data. These observations proved valuable for confirming the orbital period seen in the Calypso data (see below).

3. REDUCTION AND PHOTOMETRY

All frames were reduced in the standard way to remove instrumental artifacts. In order to minimize the impact of cosmic rays, each image was shifted to a standard reference position and co-added in the following way: first, all images were ordered in time sequence, then a running set of three

TABLE 1
OBSERVATIONS

Julian Date	Date	N_{exp}	Comments
1995 SAAO *V*-Band Data			
2,449,833.....	Apr 25	11	Outburst decline
2,449,835.....	Apr 27	21	Outburst decline
2,449,837.....	Apr 29	19	
2,449,838.....	Apr 30	18	
2,449,839.....	May 1	16	
2001 Calypso *I*-Band Data			
2,451,988.....	Mar 20	1	
2,451,990.....	Mar 22	3	
2,451,992.....	Mar 24	1	
2,451,994.....	Mar 26	2	
2,451,999.....	Mar 31	1	
2,452,026.....	Apr 27	27	
2,452,028.....	Apr 29	13	Outburst rise?
2,452,050.....	May 21	17	
2,452,051.....	May 22	19	
2,452,052.....	May 23	23	
2,452,053.....	May 24	23	
2,452,054.....	May 25	34	
2,452,055.....	May 26	29	
2,452,056.....	May 27	19	
2,452,058.....	May 29	38	
2,452,059.....	May 30	52	
2,452,060.....	May 31	32	
2,452,084.....	Jun 24	29	
2,452,086.....	Jun 26	3	
2,452,087.....	Jun 27	36	Outburst rise
2,452,088.....	Jun 28	23	Outburst rise
2,452,089.....	Jun 29	21	Outburst rise
2,452,090.....	Jun 30	15	Outburst rise

NOTE.—All observations are in quiescence unless otherwise noted.

images was co-added from the beginning to the end of the night, incremented by one image at a time. This produced a smoothing of the light curve, but kept the time sampling interval at roughly the exposure time of the individual images (plus read time).

The co-added frames were photometered using the APPHOT package in IRAF (Tody 1986). A set of isolated, well-exposed stars near V101 with low variability ($\leq$0.02 mag) was used to tie all the epochs together onto the same instrumental magnitude system. Calibration was achieved by comparing our instrumental magnitudes with Peter Stetson's photometry of M5[2] (Stetson 2000) in the *I* and *V* bands. Because of the small fields of the Calypso and SAAO detectors, the calibration was bootstrapped to the Stetson standards through intermediate wider field images taken under photometric conditions. A wide-field *I*-band image of M5 taken with the 8K mosaic camera, on the Hiltner 2.4 m telescope, at the MDM Observatory, on 2001 June 1, by J. D. N. was used to bootstrap the Calypso photometry. The SAAO photometry was bootstrapped using a *V*-band image kindly taken for us by Ron Downes with the T1KA camera on the 2.1 m telescope at Kitt Peak National Observatory on 1998 May 28. In each case and at each step, at least 25 stars were used, and a final absolute photometric calibration of better than 0.1 mag was achieved for all photometry. The final calibrated *I*-band magnitudes are presented in Table 2, and the final calibrated *V*-band magnitudes are presented in Table 3.

[2] Available at http://cadcwww.dao.nrc.ca/cadcbin/wdb/astrocat/stetson.

TABLE 2
CALYPSO *I*-BAND PHOTOMETRY

Julian Date	*I* (mag)	Error (mag)
2,451,988.938	20.34	0.03
2,451,990.986	20.05	0.04
2,451,990.995	20.11	0.05
2,451,991.002	20.17	0.06
2,451,992.882	20.13	0.03
2,451,994.914	20.18	0.03
2,451,994.925	20.24	0.03
2,451,999.937	20.34	0.06
2,452,026.752	19.67	0.04
2,452,026.760	19.93	0.04
2,452,026.767	19.88	0.03
2,452,026.774	19.96	0.03
2,452,026.781	19.92	0.03
2,452,026.789	19.91	0.03
2,452,026.804	19.90	0.03

NOTES.—Table 2 is presented in its entirety in the electronic edition of the Astronomical Journal. A portion is shown here for guidance regarding its form and content.

The *I*-band photometry is summarized in Figure 2 with a single night during quiescence shown in Figure 3 to illustrate a typical night's *I*-band light curve. The *V*-band photometry is summarized in Figure 4 and a single night's *V*-band observations during quiescence are shown in Figure 5. Figure 2 shows what may be the beginning of an outburst on JD 2,452,028 and one well-observed outburst rise starting at JD 2,452,087. Figure 4 shows a decline from outburst to a *V* magnitude of 22.0 on JD 2,449,837.

TABLE 3
SAAO *V*-BAND PHOTOMETRY

Julian Date	*V* (mag)	Error (mag)
2,449,833.436	19.78	0.04
2,449,833.447	19.81	0.04
2,449,833.459	19.83	0.04
2,449,833.469	19.81	0.03
2,449,833.500	19.82	0.04
2,449,833.530	19.85	0.04
2,449,833.560	19.83	0.03
2,449,833.573	19.83	0.04
2,449,833.594	19.84	0.04
2,449,833.615	19.87	0.05
2,449,833.634	19.90	0.05
2,449,835.374	20.53	0.04
2,449,835.386	20.57	0.04
2,449,835.397	20.67	0.04
2,449,835.408	20.68	0.05

NOTES.—Table 3 is presented in its entirety in the electronic edition of the Astronomical Journal. A portion is shown here for guidance regarding its form and content.

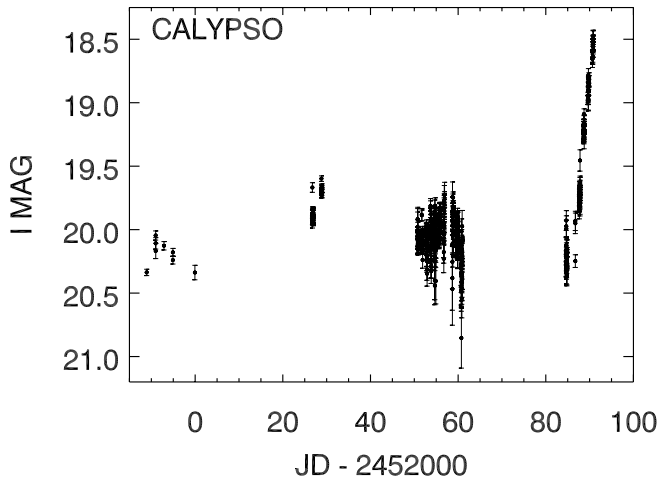

FIG. 2.—Calypso photometry summarized showing the individual *I*-band observations.

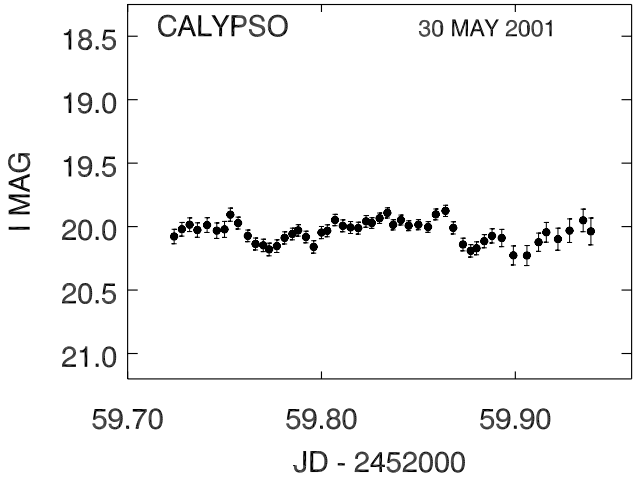

FIG. 3.—One night from the Calypso observations during quiescence showing the "flickering" typical of CVs.

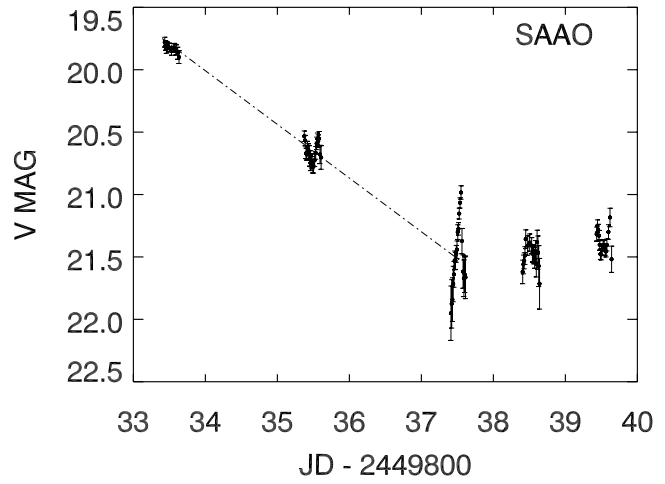

FIG. 4.—SAAO photometry summarized showing the individual *V*-band observations. The empirical relation between orbital period and outburst decline rate from eq. (3.5) of Warner (1995) is overplotted as a dot-dashed line (see § 5.1).

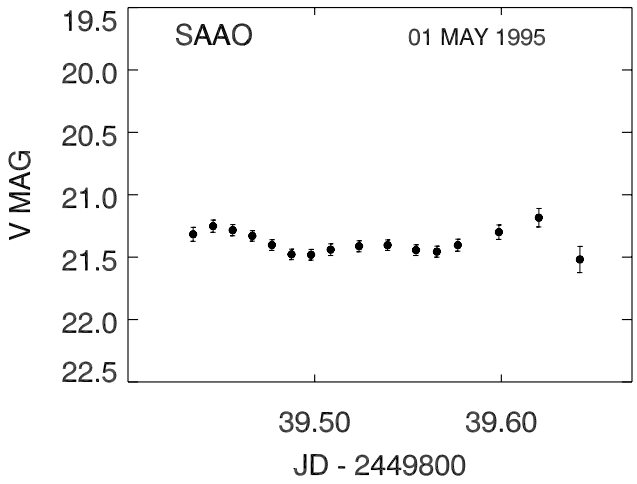

FIG. 5.—Same as Fig. 3, but for the SAAO observations during quiescence.

4. ORBITAL PERIOD ANALYSIS

To derive the orbital period, we used the algorithm of Scargle (1982) and Horne & Baliunas (1986), accelerated by the technique described in Press & Rybicki (1989). The calibrated magnitudes were converted to flux units for the period analysis. Residual long-term trends were removed by taking each night, calculating the mean flux for the night, and subtracting this mean flux from the individual fluxes from the night.

4.1. *Calypso Data*

We used all data with errors ≤ 0.2 mag to generate the periodogram shown in Figure 6. The most significant peak is at $\omega(1/d) = 8.281 \pm 0.026$ ($P = 2.898 \pm 0.009$ hr). The half-width of the periodogram peak at 85% of its peak value was used to derive all frequency error estimates in this paper.

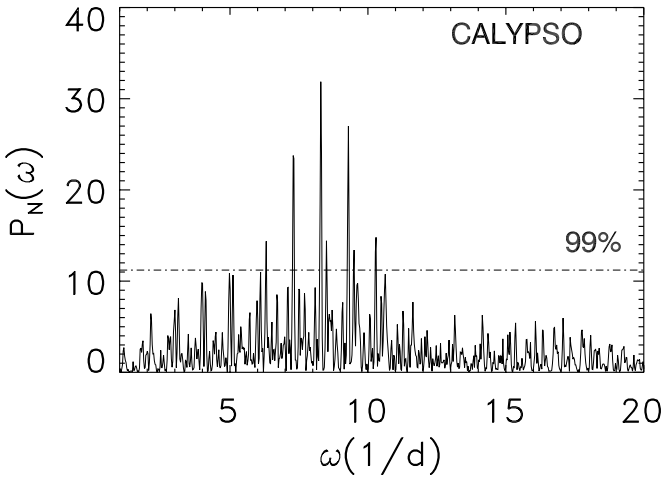

FIG. 6.—Periodogram generated from the Calypso data with errors ≤ 0.2 mag. The line of 99% confidence (false-alarm probability $= 10^{-2}$) is indicated as a dot-dashed line. The largest peak is at $\omega(1/d) = 8.281 \pm 0.026$ ($P = 2.898 \pm 0.009$ hr) and has a false-alarm probability of $10^{-10.9}$. All other significant peaks have corresponding peaks in the alias periodogram shown in Fig. 9 and are aliases because of the time sampling of the Calypso data (see § 4.1).

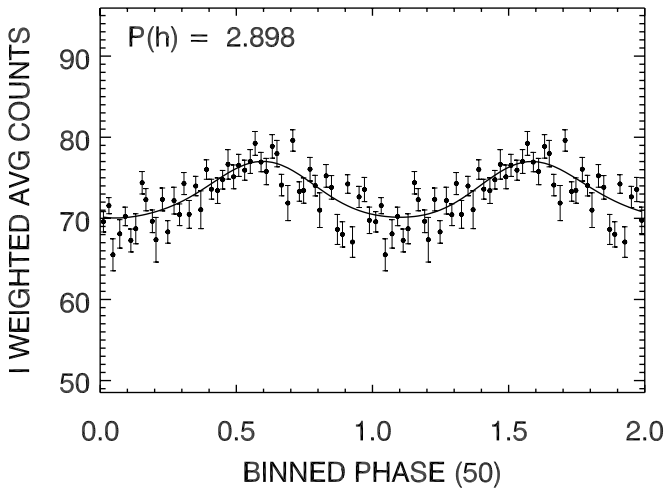

FIG. 7.—Phase diagram generated from error-weighted counts in 50 phase bins using the period of the largest peak in the Calypso periodogram. The solid line is the fit of eq. (1) to the phase points and is used to generate the alias periodogram shown in Fig. 9. The fit has a reduced χ^2 of 2.15.

If the periodic signal is due to the ellipsoidality effect (Bochkarev, Karitskaya, & Shakura 1979), then the period found in the periodogram is half the orbital period because there are two modulations per orbit. In the *I* band, this would be especially true, since the low-mass MS secondary would be prominent. An odd-even effect, where one modulation is deeper than the other, is expected because the two sides of the secondary are unequally luminous either because of gravity darkening or heating by the primary. This plus the radial velocity curve published by Naylor et al. (1989), which indicates an orbital period of $\geq$3.5 hr, motivated us to explore both the peak frequency from our periodogram and half this frequency: $\omega(1/d) = 4.140 \pm 0.026$ ($P = 5.796 \pm 0.036$ hr).

We produced the binned phase diagrams shown in Figures 7 and 8 using the error-weighted mean counts within each of 50 phase bins. Figure 8 clearly shows the expected odd-even effect of two unequal modulations per orbital

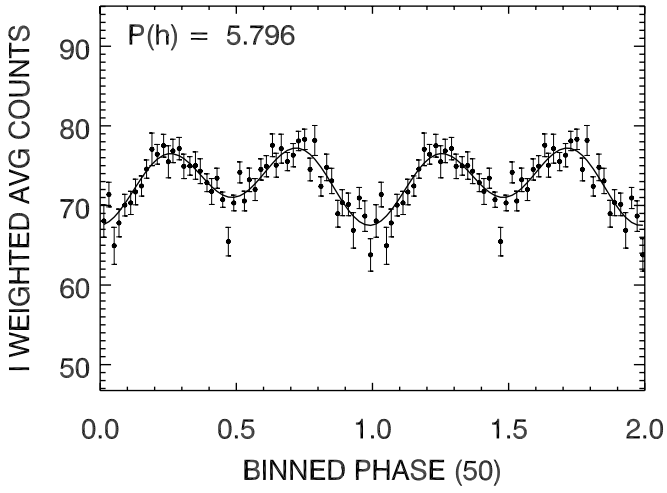

FIG. 8.—Same as Fig. 7, but using twice the period of the largest peak in the Calypso periodogram. The solid line is the fit of eq. (1) to the phase points and is used to analyze the orbital inclination of V101 (see § 5.2). The fit has a reduced χ^2 of 1.25.

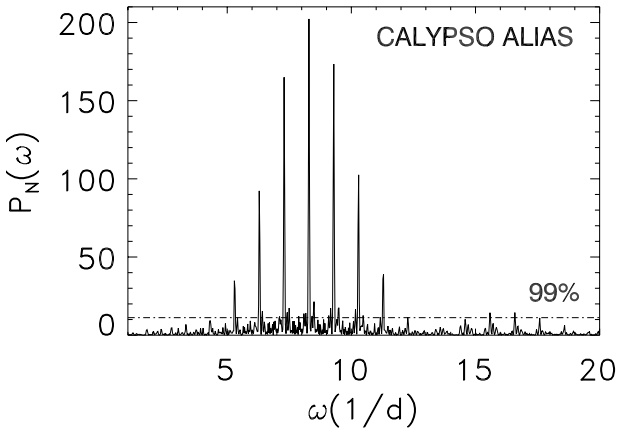

FIG. 9.—Same as Fig. 6, but for the fit in Fig. 7, sampled the same way as the Calypso observations and showing the alias peaks.

period. We fitted both sets of phase data with a periodic function of the form

$$y = a + b\cos(c\phi + d) + e\sin(f\phi + g)\ , \qquad (1)$$

where ϕ is the phase, and plotted them on the phase data. The reduced χ^2 of the fit in Figure 7 is 2.15, while that in Figure 8 is 1.25, which supports the longer orbital period.

The fit of equation (1) to the phase data was sampled the same way as the Calypso data and used to generate the alias periodogram shown in Figure 9. All significant peaks from Figure 6 have a corresponding peak in Figure 9 and apart from the highest one are aliases because of our time sampling.

4.2. *SAAO Data*

We applied the same techniques to the *V*-band data taken at the SAAO. We assumed that the orbital modulations would be present during the decline from outburst and used the run of observations from JD 2,449,833 to 2,449,839. Figure 10 presents the periodogram derived from these data.

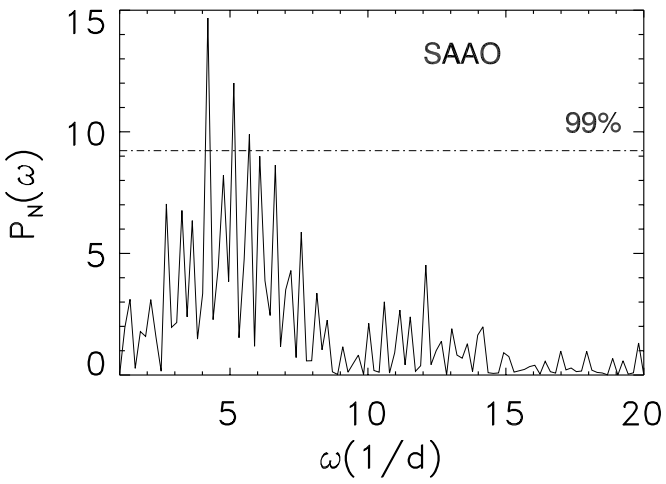

FIG. 10.—Same as Fig. 6, but for the SAAO data. The largest peak is at $\omega(1/d) = 4.20 \pm 0.19$ ($P = 5.72 \pm 0.25$ hr) and has a false alarm probability of $10^{-4.5}$.

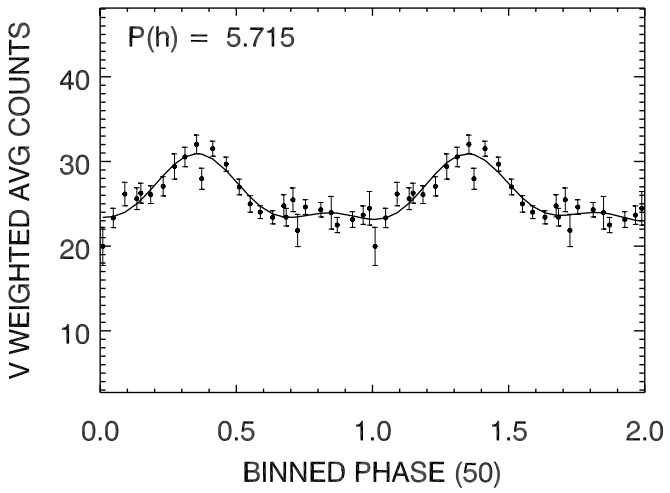

FIG. 11.—Same as Fig. 7, but using the period of the largest peak in the SAAO periodogram. The solid line is the fit of eq. (1) to the phase points and is used to generate the alias periodogram shown in Fig. 12. The fit has a reduced χ^2 of 1.09.

While this periodogram is not as clean as the periodogram derived from the Calypso data, its most significant peak at $\omega(1/d) = 4.20 \pm 0.18$ ($P = 5.72 \pm 0.25$ hr) does support the 5.796 hr period from the Calypso data. The binned phase diagram using the weighted mean counts within each of 50 phase bins is presented in Figure 11.

We also fitted this phase diagram with equation (1) in order to investigate aliases in the periodogram. The fit is presented as the solid line in Figure 11. The alias test periodogram is presented in Figure 12. Most of the significant peaks can be explained as aliases from our time sampling.

5. INTERPRETATION

5.1. *Orbital Period of V101*

The phase diagram presented in Figure 8 shows the odd-even phenomenon from the ellipsoidality effect caused by the changing geometry of the distorted secondary during the orbital cycle and the unequally luminous halves of the secondary. This effect has a small amplitude and only with many observations can the superposed stochastic variations from the accretion process be averaged out.

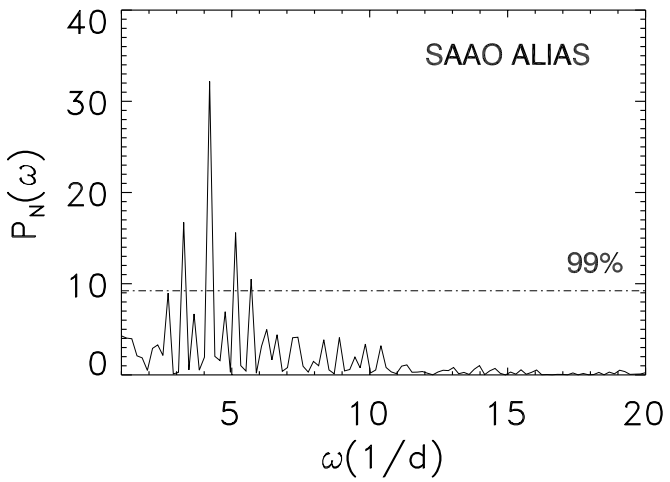

FIG. 12.—Same as Fig. 6, but for the fit in Fig. 11, sampled the same way as the SAAO observations and showing the alias peaks.

Figure 2.45 from Warner (1995), showing the observed relationship between spectral type and $P_{\rm orb}$, places the secondary of V101 in the range of spectral types from K5 to M0. This is consistent with spectral observations published by Margon et al. (1981), Naylor et al. (1989), and Shara et al. (1990), which show a red continuum in quiescence.

The phase diagram for the SAAO V-band data presented in Figure 11 shows a modulation of the same period. We expect the secondary to be much fainter in the V-band, since the secondary is of spectral type K5–M0 with $(V-I) \simeq 2.2$, and so we see only one modulation per orbit, perhaps because of the changing visibility of the primary star or the changing aspect of the accretion disk.

As a further consistency check, we compare the decay from outburst shown in Figure 4 with equation (3.5) from Warner (1995), which relates the outburst decay timescale, τ_d, to $P_{\rm orb}$:

$$\tau_d = 0.53 P_{\rm orb}^{0.84}(\text{hr}) \text{ days mag}^{-1} . \quad (2)$$

We have overplotted this relation for an orbital period of 5.796 hr on Figure 4 as a dot-dashed line, which follows the decline well. This orbital period places V101 well above the period gap for CVs and at the high end of the distribution for CVs above this gap (Warner 1995).

5.2. *Orbital Inclination of V101*

Having a constraint on the spectral type of the secondary allows us to use the light curve to explore the orbital inclination of the system using the tables in Bochkarev et al. (1979), assuming that the modulations shown in Figure 8 are purely due to the ellipsoidality effect. The fit shown in Figure 8 as the solid line and the average deviation from this fit was used to determine the amplitude of the variation ($A = 0.114 \pm 0.020$ mag), the difference between the two minima ($\Delta m = 0.055 \pm 0.021$ mag), and their corresponding errors.

Knowing that the secondary is a K5–M0 dwarf constrains the effective temperature, which, combined with the filter bandpass and the fact that the envelope of the secondary star is convective, allows us to use Figure 2 from Bochkarev et al. (1979) to determine the gravity-darkening coefficient, $\beta \simeq 0.4$. The limb-darkening coefficient is also determined by the effective temperature, and using Figure 17.6 from Gray (1976) we obtain $u \simeq 0.5$. We know that the secondary is filling its Roche lobe, so we can set the Roche lobe filling factor to be $\mu = 1$. We can also assume that the mass ratio, $q = M_p/M_s$, is in the range 1.6–2.3 by using the mass of a K7 dwarf for the secondary star mass, $M_s \simeq 0.6\ M_\odot$, and assuming the primary star mass, M_p, is in the range 1.0–1.4 $M_\odot$ (see § 5.5). Note that the q used by Bochkarev et al. (1979) is the inverse of that used traditionally in the CV literature, where $q = M_s/M_p$.

Using these values to examine Table 1 from Bochkarev et al. (1979), we can constrain the inclination angle, i, by A to be in the range $30^\circ < i < 60^\circ$. Using Table 2 from Bochkarev et al. (1979), we can constrain the inclination angle by Δm to be in the range $50^\circ < i < 90^\circ$. These two constraints overlap in the range $50^\circ < i < 60^\circ$ and are consistent with the fact that no eclipses are seen.

5.3. *Distance to V101*

We can now use the empirical relation between orbital period, $P_{\rm orb}$, and secondary luminosity, $M_V(2)$, to determine the distance modulus to V101. Using equation (2.102) from Warner (1995),

$$M_V(2) = 16.7 - 11.1 \log P_{\rm orb}(h) \ , \quad (3)$$

we determine the absolute magnitude of the secondary to be $M_V = +8.2$. Figure 2.46 in Warner (1995) shows that the scatter in this relation is about ± 0.5 mag. From the minimum published V magnitude of 22.5 (Kukarkin & Mironov 1970) and $M_V = +8.2$, we obtain a distance modulus of $(m - M)_V = 14.3 \pm 0.5$, consistent with the distance modulus of M5 of $(m - M)_V = 14.41 \pm 0.07$ (Sandquist et al. 1996).

5.4. *Outburst Period of V101*

If the rise seen in Figure 2 on JD 2,452,028 is indeed the beginning of an outburst, then the two outbursts we observe separated by 60 days with an intervening quiescent period supports the outburst period first proposed by Oosterhoff (1941) of 66 days. Many observations of individual outbursts have been reported (Margon et al. 1981; Shara et al. 1987; Naylor et al. 1989). Using these data to examine the periodicity of the outbursts shows that no regular period for the outbursts exists, but a "typical" outburst interval is in the range of 60–66 days. This is expected behavior for DN outbursts that do not exhibit strict periodicity. The observations reported by Kaluzny et al. (1999) also show two outbursts with an intervening quiescent period separated by 66 days.

5.5. *Mass and Location of V101*

A recent mass–spectral type study (Baraffe & Chabrier 1996) concludes that an M0 star has a mass of 0.6 $M_\odot$. The mass–orbital period relation, equation (2.100) from Warner (1995),

$$M_1(2) = 0.065 P_{\rm orb}^{5/4}({\rm hr}), \quad 1.3 \ {\rm hr} \leq P_{\rm orb} \leq 9 \ {\rm hr} \ , \quad (4)$$

yields 0.58 $M_\odot$ as the secondary mass of a CV with a 5.796 hr period. These are consistent with the 0.6 $M_\odot$ derived earlier from the system luminosity (and type K5–M0) near minimum. The white dwarf mass of V101 must then be greater than 1 $M_\odot$ or so to prevent dynamical mass transfer, implying a system mass in excess of 1.6 $M_\odot$. This system mass is twice that of the main-sequence turnoff in M5, which should place V101 in the inner one or two core radii of the cluster.

M5 V101 stubbornly refuses to conform to this logic. It is, in fact, located 10 core radii from the center of M5. What is it doing out there? Perhaps the simplest explanation is dynamics.

Stars lead extremely promiscuous lives in clusters, especially near the centers, where stellar densities are highest. Mate swapping is commonplace, as are strong, close encounters between binaries and single stars (e.g., Hurley & Shara 2002). These encounters often lead to the high-speed recoils of the emerging binary and single stars. Such a scenario could place V101 far from the core of M5. It also makes the intriguing prediction of the existence of a low-mass M dwarf on the opposite side of M5, considerably farther out than 10 core radii, escaping the cluster at high speed.

6. CONCLUSIONS

We conclude that the orbital period for V101 is $P = 5.796 \pm 0.036$ hr. Using this orbital period to determine a distance modulus yields $(m - M)_V = 14.3 \pm 0.5$, which supports the membership of V101 in M5. We conclude that the secondary of V101 is a low-mass MS star whose spectral type is in the range K5–M0. We also conclude that the orbital inclination is high, but not high enough for the system to exhibit eclipses.

For the generous allocation of observing time for this project, as well as material and intellectual support, we are indebted to the Calypso Observatory Director, Edgar O. Smith. We acknowledge the enthusiastic support of our engineers, Bruce Truax and Frank Scinicariello, who made this project possible. J. D. N. would like to acknowledge many useful conversations with Joe Patterson concerning methods for analyzing the periodic signal in photometric data. M. M. S. and D. A. H. B. gratefully acknowledge a generous grant of telescope time at the SAAO 1.9 m.

REFERENCES

Baraffe, I., & Chabrier, G. 1996, ApJ, 461, L51
Bochkarev, N. G., Karitskaya, E. A., & Shakura, N. I. 1979, Soviet Astron., 23, 8
Gray, D. F. 1976, The Observation and Analysis of Stellar Photospheres (New York: Wiley)
Grindlay, J. E., Heinke, C., Edmonds, P. D., & Murray, S. S. 2001, Science, 292, 2290
Hakala, P. J., Charles, P. A., Johnston, H. M., & Verbunt, F. 1997, MNRAS, 285, 693
Horne, J. H., & Baliunas, S. L. 1986, ApJ, 302, 757
Hurley, J. R., & Shara, M. M. 2002, ApJ, 565, 1251
Kaluzny, J., Thompson, I., Krzeminski, W., & Pych, W. 1999, A&A, 350, 469
Knigge, C., Shara, M. M., Zurek, D. R., Long, K. S., & Gilliland, R. L. 2002, in ASP Conf. Ser. 263, Stellar Collisions, Mergers, and their Consequences, ed. M. M. Shara (San Francisco: ASP), in press
Kukarkin, B. V., & Mironov, A. V. 1970, AZh, 47, 1211
Margon, B., Downes, R. A., & Gunn, J. E. 1981, ApJ, 247, L89
Naylor, T., et al. 1989, MNRAS, 241, 25P
Oosterhoff, P. T. 1941, Ann. Sternw. Leiden, 14 (4), 1
Pooley, D., et al. 2002, ApJ, in press
Press, W. H., & Rybicki, G. B. 1989, ApJ, 338, 277
Sandquist, E. L., Bolte, M., Stetson, P. B., & Hesser, J. E. 1996, ApJ, 470, 910
Scargle, J. D. 1982, ApJ, 263, 835
Shara, M. M., Potter, M., & Moffat, A. F. J. 1987, AJ, 94, 357
———. 1990, AJ, 99, 1858
Stetson, P. B. 2000, PASP, 112, 925
Tody, D. 1986, Proc. SPIE, 627, 733
Warner, B. 1995, Cataclysmic Variable Stars (Cambridge: Cambridge Univ. Press)